

Ultraslow \bar{p} -H collisions in hyperspherical coordinates: Hydrogen and protonium channels

B. D. Esry*

Department of Physics and J.R. Macdonald Laboratory, Kansas State University, Manhattan, Kansas 66506

H. R. Sadeghpour†

Institute for Theoretical Atomic and Molecular Physics, Harvard-Smithsonian Center for Astrophysics, 60 Garden Street, Cambridge, Massachusetts 02138

(Received 4 May 2001; published 14 January 2003)

The collision of an antiproton and a hydrogen atom at ultralow energies is described in hyperspherical coordinates. An adiabatic approximation leads to potential-energy curves that can be used to describe the dynamics of capture in the \bar{p} -H($1s$) collision. A unified formulation of the collision and capture processes leading to formation of $p\bar{p}$ bound states emerges. Both Pn(nl)- e^- “atomic-type” and \bar{p} -H($n'l'$) “molecular-type” states are represented. These potential curves are calculated to more than 10 000 protonium Bohr radii, where low-energy antiprotons are stopped in collisions with hydrogen atoms. Elastic and inelastic partial and total protonium formation cross sections in the mass-scaled \bar{p} -H system are calculated. The existence of protonium negative (or positive) ion in its ground and excited states is discussed.

DOI: 10.1103/PhysRevA.67.012704

PACS number(s): 34.90.+q, 36.10.-k, 31.50.Gh, 31.15.Ja

I. INTRODUCTION

Antiproton (\bar{p}) collisions with matter occupy a unique place in atomic collision studies. An antiproton can substitute for an electron in the atom, thereby forming an exotic system. The charge-conjugate process (proton on antihydrogen) also leads to the production of exotic systems. The deexcitation or cascade of an antiprotonic system from highly excited Rydberg states usually results in emission of energetic x rays. The existence of such exotic systems was first predicted by Fermi and Teller [1] to explain the stopping of negative muons in light elements. Recent measurements on the decay of antiprotons in helium demonstrated the existence of long-lived (microsecond lifetimes) systems [2]. A new generation of experiments with antiprotons [3] (the antiproton decelerator experiments) herald an era of low-energy \bar{p} atomic physics. Ultraslow antiproton beams with energies of the order of 10 eV, collected from Penning-type traps, are planned. Collisions with target gases at such low energies can lead to sizable formation of $p\bar{p}$ Rydberg species that can be probed with lasers. Such precise spectroscopy of protonium in high Rydberg states is scheduled, where two-photon transitions, $\lambda \sim 600$ nm, between states of principal quantum numbers $n_i \sim 35$ –45 and $n_f \sim 50$ –65 are induced. Due to low densities in the beam, Stark mixing of protonium angular momentum levels, which rapidly facilitates annihilation, is minimized allowing ample time for determination of transition frequencies and hence the Rydberg constant for the protonium. Protonium is the simplest hadronic form of neutral matter.

The most likely condition for the initial capture of an \bar{p} by an atom or a molecule is perceived to be via an energy matching or resonant condition [4], in which the \bar{p} loses

enough energy in the collision process to match the energy of the ground-state electron in the atom, $\bar{p} + \text{H}(1s) \rightarrow \text{Pn}(nl) + e^-$. For antiprotons, this matching condition translates to an initial protonium (Pn) principal quantum number, $n \sim \sqrt{\mu_{p\bar{p}}} \approx 30$, where $\mu_{p\bar{p}}$ is the reduced mass of the $p\bar{p}$ complex. For incident antiproton with energy 10 eV, the most probable initial population of protonium is in the range $n \sim 59$ –60.

Excited antiprotonic systems may decay via radiative or radiationless pathways. Radiative lifetimes of Rydberg states of antiprotonic systems, following capture by noble-gas atoms, have been observed [5] to be of the order of microseconds. The decay can also occur through interaction with atomic electrons leading to emission of Auger electrons in the cascade of \bar{p} to lower orbitals, and ultimately through strong interaction with the nucleus leading to annihilation. Determination of the Auger rates, in $\text{He}^+\bar{p}$, for instance, is important for calculating the fraction of long-lived \bar{p} in matter [6]. For the Auger process to proceed efficiently, the electron and the antiproton in $\text{He}^+\bar{p}$ must strongly interact. The long lifetimes for these systems are thus cited as an evidence for slow Auger rates for high n values [6]. Accordingly, it is thought that the antiprotons are captured in high circular states with $l \sim n - 1$. Low orbital angular-momentum states ($l \leq 2$) are prone to rapid annihilation.

Antiproton and negative muon capture processes have been of both fundamental and practical interest [7,8] as they provide substantial information on nuclear charge distributions, on hadronic and leptonic masses, and on muon catalyzed fusion. Exotic hydrogen atoms are of interest for their simplicity and because they provide information about very low-energy hadron-nucleon interactions. Antiproton collision with matter at very low energies is also of importance for the formation and cooling of antihydrogen [9,10]. Considerable attention has been given to a recent detection of cold antihydrogen atoms [11,12]. High-resolution spectroscopy of Pn in

*Email address: esry@phys.ksu.edu

†Email address: hsadeghpour@cfa.harvard.edu

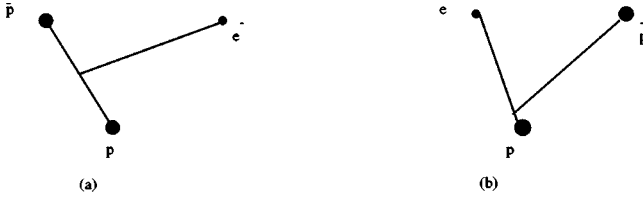


FIG. 1. The Jacobi coordinates showing (a) the protonium formation, and (b) the initial collision coordinates.

highly excited states, $Pn(n \sim 30-40)$, and the study of annihilation process depends on the knowledge of Pn level population and formation rate, in the collision of the \bar{p} beam with the target gas [3,13,14]. Cross sections for forming Pn in excited Rydberg levels provide a necessary guide for the determination of the optimal laser transition lines.

II. THEORETICAL FRAMEWORK

Calculations of Pn formation in collision of \bar{p} and hydrogen atoms are difficult, owing to the fact that the final product, protonium, can form in compact orbits compared with the orbit of the electron in hydrogen [14,15], whereas atomic electrons are bound in orbits of the order of a Bohr radius (1 Å), proton-antiproton atoms form in orbits of tens of Fermi (10^{-4} Å). For instance, the mean radius of circular orbits of Pn , with $l = n - 1$, is given by $r_n = 57.64n^2$ fm [7]. The Coulomb three-body problem in the standard Born-Oppenheimer approximation (BO) separates in spheroidal coordinates in which the \bar{p} - p distance is treated as an adiabatic parameter. The energy eigenvalues as a function of this parameter give the potential-energy curves that dissociate, for the case of \bar{p} -H, into an antiproton and an excited $H(nl)$ atom. *The formation of $Pn(nl)$ cannot be accounted for in the usual BO approximation.*

The hyperspherical coordinate method, on the other hand, offers a means for calculating processes that occur over many orders of magnitude in energy or distance. For the present application, the hyperspherical method yields both the collision channel and the capture channels into which excited Pn atoms decay. This is because the different rearrangement configurations, see Fig. 1, describing the collision of antiprotons with hydrogen atoms and the capture and decay of \bar{p} to lower protonium orbitals are formulated in a unified framework in hyperspherical coordinates. Adiabatically, we can address the existence of bound and resonant protonium negative or positive ions within the same calculation.

The uniform representation of diverse length scales, from $Pn(1s)$ to $H(1s)$, in a single approach is the hallmark of this calculation. The number of $Pn(nl)$ channels, roughly 500, available in the ultraslow collision of \bar{p} with ground-state hydrogen makes an immediate numerical multichannel calculation of formation cross section difficult. We anticipate, however, that by properly scaling the problem down to a more manageable number of states, we can glean valuable information about the capture and formation physics.

Recently, Tolstikhin, Watanabe, and Matsuzawa [16] cal-

culated a restricted set of adiabatic hyperspherical potential-energy curves for the \bar{p} -He⁺ system for large total angular-momentum states, relevant to the \bar{p} -He($2s, 2p$) collision. The objective of this work was to demonstrate the utility of the hyperspherical method and its connection to the BO approximation. They were similarly considering \bar{p} capture to high n states of the \bar{p} -He²⁺ system, but in the symmetric-top approximation, they needed to calculate only a modest number of channels.

The characteristic feature of the hyperspherical approach is the contraction of the set of infinite-extent coordinates into a single radial coordinate, the hyper-radius R . All other coordinates are collected in the interparticle angles and a set of hyperangles, written as mass-weighted ratios of independent particle coordinates. (A review of the literature on hyperspherical coordinates in Coulomb three-body systems is given by Lin [17].)

The starting point of our calculation is the Schrödinger equation for \bar{p} -H in the center of mass,

$$\left[-\frac{1}{2\mu_1} \nabla_{\rho_1}^2 - \frac{1}{2\mu_2} \nabla_{\rho_2}^2 + V \right] \Psi = E \Psi, \quad (1)$$

where the interparticle potential energy is $V = -(1/r_{p\bar{p}}) + (1/r_{\bar{p}}) - (1/r_p)$ and the Jacobi vectors ρ_1 and ρ_2 are chosen to represent the relative motion of p and \bar{p} , and the motion of the electron relative to the center of mass of the $p\bar{p}$ system, respectively, as in Fig. 1(a). The reduced masses are $\mu_1 \equiv \mu_{p\bar{p}} = m_p/2$ and $\mu_2 = 2m_p/(2m_p + 1)$, and we use atomic units throughout.

By defining a mass-weighted set of coordinates $r_1 = \sqrt{(\mu_1/\mu)}\rho_1$ and $r_2 = \sqrt{(\mu_2/\mu)}\rho_2$, a hyper-radius $R = \sqrt{r_1^2 + r_2^2}$ and a hyperangle $\alpha = \tan^{-1}(r_2/r_1)$ can be written down [17,18]. The arbitrary reduced mass μ is set equal to the geometric mean of the Jacobi reduced masses, i.e., $\mu = \sqrt{\mu_1\mu_2} \approx 30.3$. The Schrödinger equation for \bar{p} -H, when transformed into hyperspherical coordinates, reads

$$\left[-\frac{1}{2\mu} \frac{\partial^2}{\partial R^2} + \frac{\Lambda^2 + \frac{15}{4}}{2\mu R^2} + V \right] \Psi = E \Psi, \quad (2)$$

where we have eliminated the first derivatives in R and α by writing $\Psi = R^{5/2}(\sin \alpha \cos \alpha) \bar{\Psi}$. Note that the generalized angular-momentum operator Λ (written here in the body frame),

$$\Lambda^2 = -\frac{\partial^2}{\partial \alpha^2} - \frac{1}{\sin^2 \alpha \cos^2 \alpha \sin \theta} \frac{\partial}{\partial \theta} \left(\sin \theta \frac{\partial}{\partial \theta} \right), \quad (3)$$

commutes with the kinematic rotations [20], i.e., it has the same form for all choices of Jacobi coordinates. This ensures that each possible breakup channel will be reproduced in the large R limit. In this expression, θ is the angle between ρ_1 and ρ_2 . The potential energy can formally be expressed in

hyperspherical coordinates once the interparticle coordinates are given in terms of the Jacobi coordinates:

$$r_{p,\bar{p}}^2 = \frac{1}{4} \rho_1^2 + \rho_2^2 \pm \rho_1 \rho_2 \cos \theta, \quad (4)$$

where the \pm signs refer, respectively, to the $e^- - \bar{p}$ and the $e^- - p$ distances.

In the adiabatic approximation, the hyper-radius is treated as a parameter and the operator sum of the angular momentum and the potential-energy terms in Eq. (2) is diagonalized [19]. We used an expansion over a direct product of basis splines to represent the adiabatic channel functions. The eigenvalue equation was thus transformed into a generalized algebraic eigenvalue problem of approximate dimensions $10^4 \times 10^4$ (~ 185 functions in α and 50 functions in θ). The distribution of splines was adjusted as a function of R to account for the collapse of the channel functions into the attractive potential wells. In particular, a large fraction of the splines in α were needed just to represent the polarized $p\bar{p}$ hydrogenic functions up to $n \sim 30$. A considerable fraction of the remaining functions were packed near the $e^- p$ coalescence point [$\alpha_0 = \tan^{-1}(1/\sqrt{2m_p + 1})$, $\theta = 0$] to represent the $H(1s)$ function.

The resulting eigenvalues $U_\nu(R)$ span the discrete- and continuous-energy spectra in the collision of an antiproton and a hydrogen atom. The cost of neglecting the motion in the hyper-radius, in the adiabatic approximation, is manifested in the first- and second-order coupling of the adiabatic channels. These coupling matrix elements are, respectively, $P_{\lambda\nu} = \langle \phi_\lambda | \partial/\partial R | \phi_\nu \rangle$ and $Q_{\lambda\nu} = \langle \phi_\lambda | \partial^2/\partial R^2 | \phi_\nu \rangle$, where ϕ_ν are eigenvectors from the diagonalization of the adiabatic Hamiltonian. These couplings are responsible for all inelastic processes.

III. RESULTS: PROTONIUM FORMATION

Figure 2 gives the adiabatic potential-energy curves, $U_\nu(R)$, as a function of the hyper-radius R for forming protonium atoms in ground and excited Rydberg states, $Pn(nl)$. The potentials are shown as a function of an effective protonium quantum number, $\nu(R) = [-2U_\nu(R)]^{-1/2}$, which at large R tends to the principal protonium quantum number $\nu(R \rightarrow \infty) = n$. These curves have been calculated up to $R \sim 80$ a.u., but are shown here to $R \sim 65$ a.u. We note that the conversion factor to protonium atomic units is $\sqrt{\mu_{p\bar{p}}}\mu$ so that $R \approx 80$ a.u. corresponds to $\approx 13\,300$ Pn units. A potential ridge forms near $\alpha \sim 0$, corresponding to the $\bar{p}-p-e^-$ arrangement.

As noted previously, there are two possible bound systems in the collision of \bar{p} and H: $Pn(nl)$ and $H(n'l')$. The asymptotic potential-energy curves shown in Fig. 2 represent both the $\bar{p}-H(n'l')$ “molecular-type” states and the $Pn(nl)$ “atomic-type” states. Due to the degeneracy of orbital angular-momentum levels, both $H(n'l')$ and $Pn(nl)$ states become Stark mixed in the presence of the external field of the antiproton and the electron, respectively. The resulting induced dipole moments can be attractive and repulsive; only

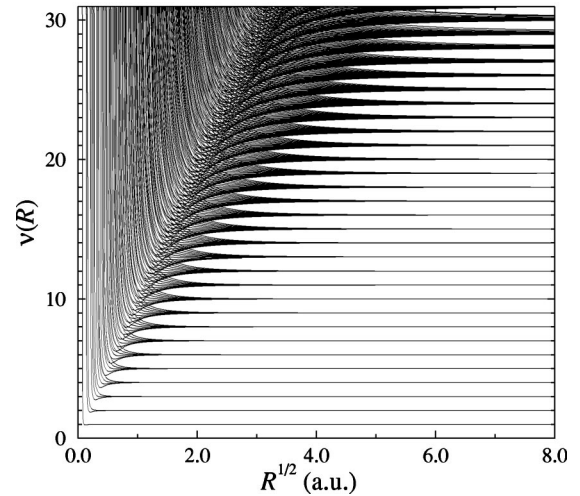


FIG. 2. The \bar{p} -H (or $p\text{-}\bar{H}$) adiabatic hyperspherical potential curves as a function of the square root of R . The curves are shown on an effective quantum number $\nu(R)$ scale to separate out the asymptotic hydrogenic protonium channels. All curves for zero total angular momentum leading up to $n=30$ are displayed.

hydrogen or protonium negative-ion channels with attractive dipole moments may support bound levels.

Although the incoming collision channel, $\bar{p} + H(1s)$ is represented in this calculation, due to large \bar{p} p reduced mass, it is not easily discerned in this figure. Only when the potential curves are expanded in the range of $R > 30$ a.u. and in the vicinity of the $n=30$ manifold, does the collision channel appear, as shown in Fig. 3. The adiabatic hyperspherical calculation confirms that the most likely principal quantum number for the initial formation of $Pn(n)$ in the low-energy collision of \bar{p} with H to be $n=30$. In the present formalism with zero total angular momentum, about 465 protonium formation channels are available to the antiproton. The most favorable capture transitions are likely those that maximize the overlap of the final channel wave functions with the initial continuum wave function. One thus expects the initial $(\bar{p}-p-e^-)$ complex at low incident energies to form in high principal quantum numbers, $n \sim 30$ [21]. This complex then cascades due to the coupling of the adiabatic channels via $P_{\lambda\nu}$ and $Q_{\lambda\nu}$ to lower-lying Pn states, in addition to the usual radiative pathways.

The Stark mixing of the orbital angular-momentum levels in each n manifold induces point dipoles with strength a_ν in each Pn channel ν [22]. When $a_\nu < -\frac{1}{4}$ a.u., the effective potential $U_{eff}(R) = U_\nu(R) - (1/2\mu)Q_{\nu\nu}(R)$ supports an infinite number of resonant states converging exponentially to each $Pn(n)$ threshold. In the $n=2$ manifold, the attractive dipole moment is about -2×10^{-5} a.u., not large enough to bind an electron. In fact, only when the protonium is excited to $n \geq 30$, would we expect the electrons to bind. This expectation follows from the fact that the effective point dipole moments scale roughly as $3n^2$ [23]. Hino and Macek [24] showed that the $dt\mu$ system, due to its floppiness, has sufficiently large dipole moments in the $n=2$ manifold to bind

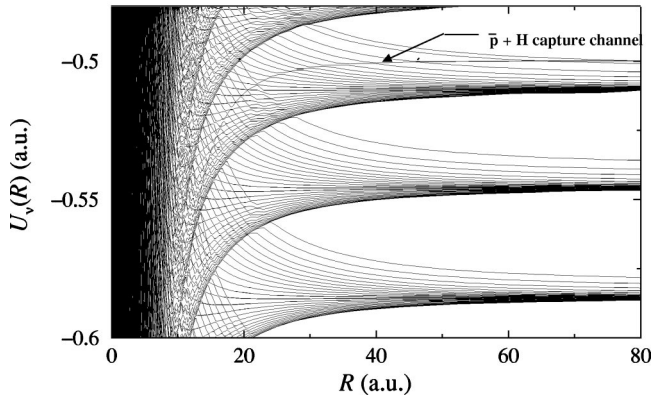


FIG. 3. An expanded snapshot of the adiabatic potential curves in Fig. 1, near the $\text{Pn}(n=30)$ threshold. The initial collision channel is shown by an arrow. The curves converging to $\text{Pn}(n=28,29)$ are also shown.

muons into an infinity of resonant states and to produce observable oscillations above the $t\mu(d\mu)$ $n=2$ threshold. Similar resonances have been argued [25] to play a role in explaining the smaller-than-expected measured muon cycling rate.

In the ground state of protonium, first-order Stark mixing is absent, and the second-order mixing is expected, on physical grounds, to lead to an attractive polarization potential. In the adiabatic hyperspherical approximation, on the other hand, the long-range form of the effective ground-state potential energy contains a repulsive polarization potential that has the form [26]

$$U_{eff}(R) \rightarrow -\frac{m_p}{4} + \frac{3(2m_p+1)}{8m_p^3 R^4} \left[1 - \frac{48}{m_p^2} \right], \quad \text{as } R \rightarrow \infty. \quad (5)$$

This expression shows that the polarization potential in the ground state in hyperspherical coordinates becomes repulsive for large particle masses. Our ground-state effective potential in Fig. 4 clearly shows this repulsive behavior, agreeing with Eq. 5 to at least three significant digits. In fact, only for $m'_p < \sqrt{48}$ (see below), is the polarization potential attractive. Incorporation of nonadiabatic coupling in a coupled-channel calculation effectively restores the correct asymptotic form to the potential.

Since the electric dipole polarizability scales as $\alpha_{\text{Pn}} = \alpha_{\text{H}}/\mu_{pp}^3$, it is expected that an electron cannot bind to $\text{Pn}(1s)$. The potential curve in Fig. 4 (solid line), however, contains at least one bound state at energy -459.102 a.u. (the threshold is at $-m_p/4 = -459$ a.u.). Because the potential does not include the diagonal correction, this energy is a rigorous lower bound to the exact ground-state energy. When the diagonal correction $Q_{11}(R)$ is added, providing a rigorous upper bound on the exact ground-state energy, the resulting potential is no longer deep enough to support a bound state. From Eq. 5, however, it is clear that a single-channel calculation does not incorporate all of the correct physics. A coupled-channel calculation confirms that the protonium

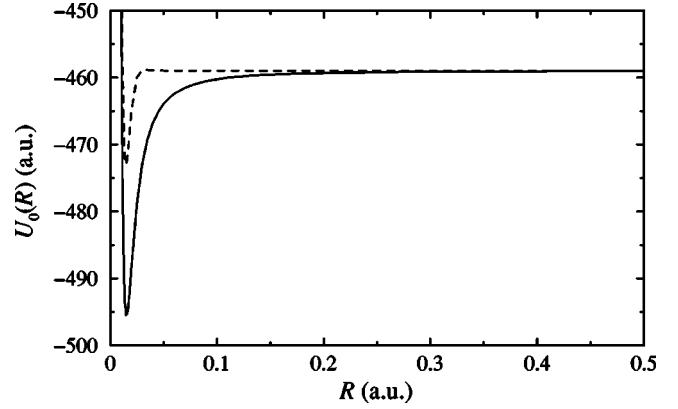


FIG. 4. The adiabatic hyperspherical channel for $\text{Pn}^-(1s)$ is shown. It supports one bound state at -459.102 a.u. The dashed curve includes the diagonal correction and does not contain bound states.

atom in the ground state indeed is not able to bind an electron, in line with the arguments given by Lin [17] and Frolov [27]. It is worth mentioning that the diagonal correction to the lowest adiabatic channel, $Q_{11}(R)$, is $-(3/4R^2)$ to leading order in R^{-1} as $R \rightarrow \infty$. This value is in accord with the analytic result, $R^2 Q_{11}(R) = -\frac{1}{4} + \langle u_{10} | r^2 | d^2 u_{10} / dr^2 \rangle - \langle u_{10} | r | du_{10} / dr \rangle$ [19], where $u_{10}(r)$ is the usual unpolarized radial wave function for $\text{Pn}(1s)$.

A calculation involving nearly 500 coupled adiabatic channels is prohibitive. It is, however, possible to exploit the fact that many of the avoided crossings in Fig. 2 are sharp, i.e., the transitions are diabatic. The large degree of adiabaticity should offer savings in terms of reduction in the number of physically relevant channels. But, because there does not exist a good prescription for obtaining these dominant diabatic potential curves, we opt to reduce the number of physical channels by artificially scaling the proton mass. In this manner, one may identify systematic trends in the cross sections, as a function of mass m'_p (the prime will be used to indicate mass-scaled quantities). The proton mass has been scaled to place the entrance channel above a given protonium threshold n according to

$$m'_p = \frac{2n^2(n+1)^2}{(n+1)^2 - \alpha(2n+1)} - 1. \quad (6)$$

In this expression, α is a parameter that dictates the energy separation between the H' entrance channel and the Pn' manifold as a fraction of the $\text{Pn}'(n)$ and $\text{Pn}'(n+1)$ energy splitting. For our scalings, we have taken $\alpha=0.1$ as is approximately true for the physical \bar{p} -H system. In addition to the mass-scaling feature, it is possible to make general remarks about certain propensity rules for this system. We find that, throughout, the most dominant channels contributing to the formation of protonium levels are the lowest adiabatic dipole channels in each $\text{Pn}'(n)$ manifold. A physical interpretation for this propensity rule is that the most attractive induced dipoles form that point toward the electron, while keeping the \bar{p} on the other side of the electron. This configuration minimizes the total energy and interacts most strongly

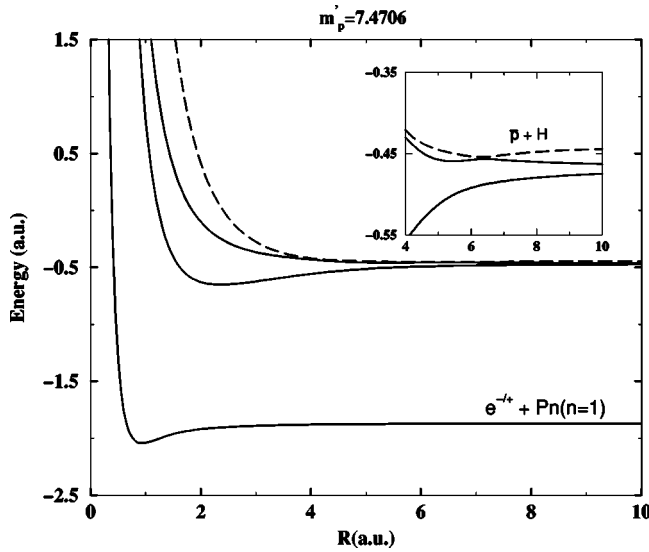


FIG. 5. The adiabatic potential-energy curves for the collision \bar{p} -H, with a proton mass $m_p' = 7.4706$.

with the \bar{p} -H channel. This observation is corroborated by studying the coupling matrix elements, as they scale with mass m_p' , and with the adiabatic index for the lowest adiabatic potential, ν_m , for each mass. Using these systematic trends, we anticipate to be able to draw qualitative conclusions about the formation of Pn levels.

As an illustrative example, Fig. 5 gives the adiabatic potential curves for the mass-scaled case, $m_p' = 7.4706$. The initial collision channel is shown in the inset, and a total of four energetically accessible channels are included in the scattering calculation. Figure 6(a) gives the corresponding protonium formation partial [Pn'(n=1,2)] and total cross sections. Over the energy range considered, the dominant formation channel is the lowest dipole channel, labeled Pn'(2s) for convenience. Near the entrance channel threshold, the formation of protonium in the next lowest dipole potential in the Pn'(n=1) manifold also becomes large. The behavior of the total Pn formation cross section at ultra low energies is $\epsilon^{-1/2}$, where ϵ is the kinetic energy of the incident \bar{p} —in accordance with the Wigner threshold behavior [28]. The elastic \bar{p} -H cross section approaches a constant value as $\epsilon \rightarrow 0$, also an expected threshold behavior. The same pattern is repeated for a higher mass scaling, $m_p' = 17.824$ in Fig. 6(b). The cross section for Pn formation drops as the system becomes heavier. The total number of adiabatic channels that become energetically available is seven for the $m_p' = 17.824$ case. [In both coupled-channel calculations, the total number of retained channels is 30, sufficient to obtain convergence in the number of energetically closed channels.] It is noted that the cross sections in Fig. 6 are calculated for zero total angular momentum. At energies near $\epsilon \sim 10^{-3}$ for the $m_p' = 7.4706$ case, three partial waves, $J=0, 1$, and 2 contribute to the total elastic cross section. At lower energies, the contribution from all but the lowest, i.e., $J=0$, will become negligible. Based on these calculations, we anticipate that the process of protonium formation in the

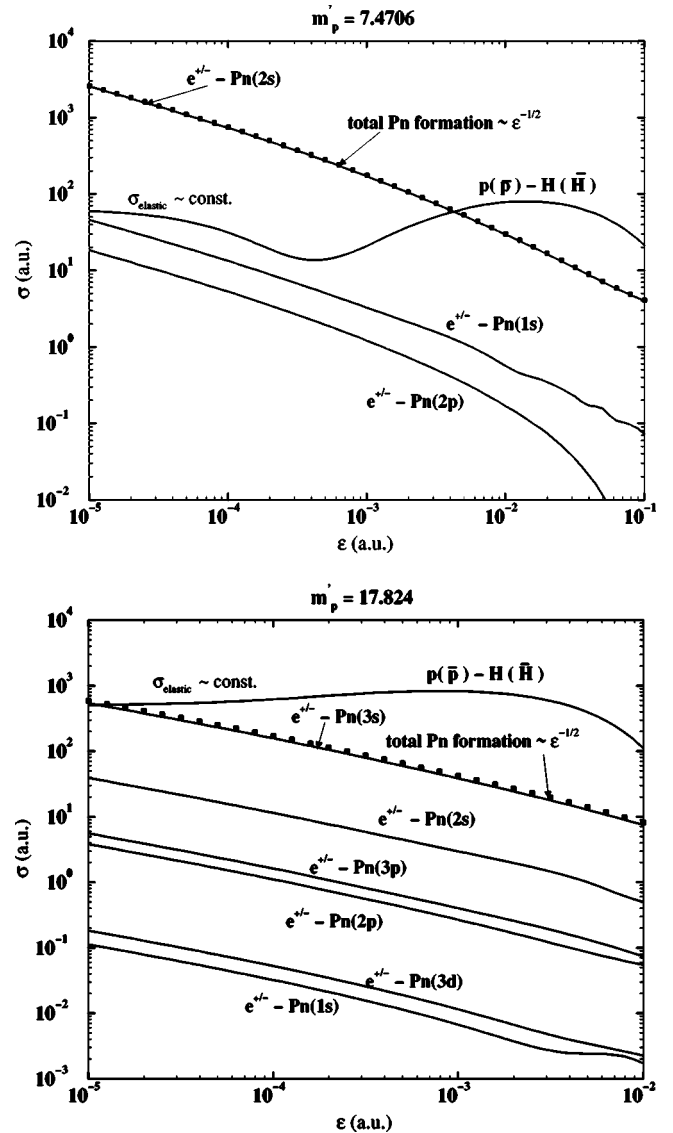


FIG. 6. The elastic and inelastic partial and total protonium formation cross sections as a function of the incident energy, for the mass-scaled \bar{p} -H problem with (a) $m_p' = 7.4706$ and (b) $m_p' = 17.824$. The exothermic formation cross sections behave like $\epsilon^{-1/2}$, as expected, and the elastic \bar{p} -H cross section approaches a constant at very low energies. The Pn levels refer, here, to the lowest dipole channel in each Pn(n) manifold.

collision of \bar{p} and H will be influenced by the interaction of the lowest channel in each Pn(n) manifold with the entrance \bar{p} -H channel and that protonium will be formed most prominently in the highest Pn(ns) levels.

We mention that a recent classical-trajectory Monte Carlo calculation of \bar{p} capture on H [14] finds a protonium cross section of about 70 a.u. at $\epsilon = 0.01$ a.u. By solving a set of coupled Faddeev-type equations to obtain elastic and Pn formation scattering amplitudes, Voronin and Carbonell [13] obtain Pn cross sections that scale as $\epsilon^{-1/2}$ at very low collision energies with typical values of $\sigma_{Pn} \sim 500$ a.u. near $\epsilon \sim 10^{-5}$ a.u. Although it may be tempting to compare our results for the mass-scaled cases with the above results for

the real \bar{p} -H system, we advise caution. Future investigations of the mass scaling and convergence issues remain.

IV. SUMMARY

In summary, we have calculated adiabatic hyperspherical potential-energy curves for collisions of \bar{p} on H (or p on \bar{H}) with high accuracy and to more than 10 000 protonium atomic units. Both the molecular and atomic channels, i.e., \bar{p} -H and e^- -Pn(n) channels, are calculated. At very low incident \bar{p} energies, nearly 500 channels contribute to the collision making a complete treatment of the Pn formation cross section in the adiabatic representation difficult. By scaling the mass of the heavy particles, however, we are able to reduce the number of channels involved and thus identify the dominant Pn' formation channels. We solve the coupled equations to obtain the elastic and inelastic partial and total

Pn' formation cross sections for a couple of proton masses, m'_p , and find that, as expected, the Wigner threshold law is obeyed at ultralow collision energies. In addition, we confirm that the protonium negative ion does not exist in the nonrelativistic limit, and similarly, we expect that there are no excited resonant states of the negative ion for principal quantum numbers $n < 30$.

ACKNOWLEDGMENTS

We thank Michael Cavagnero for helpful comments. Support for this work was partly provided by a National Science Foundation grant to the Institute for Theoretical Atomic and Molecular Physics at the Harvard-Smithsonian Center for Astrophysics. B.D.E. also acknowledges support from the Chemical Sciences, Geosciences and Biosciences Division, Office of Basic Energy Sciences, Office of Science, U.S. Department of Energy.

-
- [1] E. Fermi and E. Teller, *Phys. Rev.* **72**, 399 (1947).
 [2] T. Yamazaki *et al.*, *Nature (London)* **361**, 238 (1993).
 [3] T. Azuma *et al.* (ASACUSA Collaboration), proposal CERN Report No. SPSC 97-19, 1997 (unpublished); Report No. SPSC 00-04, 2000 (unpublished).
 [4] I. Shimamura, *Phys. Rev. A* **46**, 3776 (1992).
 [5] R. Bacher *et al.*, *Phys. Rev. A* **38**, 4395 (1988).
 [6] V.I. Korobov and I. Shimamura, *Phys. Rev. A* **56**, 4587 (1997).
 [7] C.J. Batty, *Rep. Prog. Phys.* **52**, 1165 (1989).
 [8] J.S. Cohen, *Phys. Rev. A* **27**, 167 (1983).
 [9] G. Gabrielse *et al.*, *Phys. Rev. Lett.* **82**, 3198 (1999).
 [10] P. Froelich *et al.*, *Phys. Rev. Lett.* **84**, 4577 (2000).
 [11] M. Amoretti *et al.*, *Nature (London)* **419**, 456 (2002).
 [12] G. Gabrielse *et al.*, *Phys. Rev. Lett.* **89**, 213401 (2002); **89**, 233401 (2002).
 [13] A.Yu. Voronin and J. Carbonell, *Phys. Rev. A* **57**, 4335 (1998).
 [14] J. Cohen, *Phys. Rev. A* **56**, 3583 (1997).
 [15] K. Sakimoto, *J. Phys. B* **33**, 3149 (2000).
 [16] O.I. Tolstikhin, S. Watanabe, and M. Matsuzawa, *Phys. Rev. A* **54**, R3705 (1996).
 [17] C.D. Lin, *Phys. Rep.* **257**, 1 (1995).
 [18] J. Macek and K.A. Jerjian, *Phys. Rev. A* **33**, 233 (1986).
 [19] J. Macek, *J. Phys. B* **1**, 831 (1968).
 [20] F. Smith, *Phys. Rev.* **120**, 1058 (1960).
 [21] J.S. Cohen, and N.T. Padial, *Phys. Rev. A* **41**, 3460 (1990); J.S. Cohen, *ibid.* **59**, 1160 (1999).
 [22] M. Gailitis and R. Damburg, *Proc. Phys. Soc. London* **82**, 192 (1963).
 [23] H.R. Sadeghpour, *Phys. Rev. A* **43**, 5821 (1991).
 [24] K. Hino and J.H. Macek, *Phys. Rev. Lett.* **77**, 4310 (1996).
 [25] P. Froelich and J. Wallenius, *Phys. Rev. Lett.* **75**, 2108 (1995).
 [26] M. Cavagnero, Z. Zhen, and J. Macek, *Phys. Rev. A* **41**, 1225 (1990).
 [27] A.M. Frolov, *Sov. Phys. JETP* **65**, 1100 (1987).
 [28] H.R. Sadeghpour *et al.*, *J. Phys. B* **33**, R93 (2000).